STOCHASTIC CONFLICT-FREE 4D TRAJECTORY OPTIMIZATION IN THE PRESENCE OF UNCERTAINTY

Yoshinori Matsuno*
*The University of Tokyo

Keywords: *air traffic management, conflict resolution, generalized polynomial chaos, response surface methodology, stochastic optimal control*

Abstract

This paper explores a near-optimal conflict-free trajectory generation algorithm to determine conflict resolution trajectories starting from any given initial states in real time without actually solving optimal control problems and sacrificing accuracy. First, the spatially correlated wind model is considered for wind uncertainty, and a probabilistic conflict detection algorithm using the generalized polynomial chaos method is proposed. The generalized polynomial chaos algorithm can determine the evolution of uncertainty in the complex nonlinear dynamical systems with high computational efficiency. In addition, a numerical algorithm that incorporates the generalized polynomial chaos method into the pseudospectral method is proposed to solve the stochastic optimal control problems. The stochastic optimal control method is combined with the proposed conflict detection algorithm to solve the conflict resolution problem. Moreover, the response surfaces of the optimal conflict-free trajectories are constructed by using the generalized polynomial chaos algorithm based on convex optimization, and the near-optimal conflict-free trajectories starting from any given initial states are generated in real time without actually solving the stochastic optimal control problems and sacrificing accuracy. Through numerical simulations of the two-dimensional conflict detection and resolution problem among multiple aircraft, the performance and effectiveness of the stochastic algorithms are evaluated and demonstrated.

1 Introduction

The air traffic demand has been growing rapidly, and current air traffic management (ATM) system is under considerable stress. To satisfy the increasing demand, the International Civil Aviation Organization (ICAO) published a new operational concept of global ATM in 2005 [1]. NextGen [2], SESAR [3] and CARATS [4] are currently ongoing in order to support the new era of air transportation. For the future ATM system, 4D trajectory based operation, defined as a precise description of an aircraft path in three-dimensional space and time, is an important concept to meet future air traffic growth. The primary concern of the ATM system is to guarantee safety, and one of the major safety critical situations is a conflict between aircraft, i.e., situation where two or more aircraft experience a loss of the minimum allowed separation. All problems in the real world contain uncertainties which arise due to disturbances, modeling and estimation errors, and aircraft also fly under various uncertainties such as unpredicted weather and navigation error. These uncertainties have effects on the aircraft motion and therefore conflict detection and resolution. Therefore, in this study, we consider the conflict detection and resolution problem in the presence of uncertainty, which is the key element for the realization of the future ATM system.

Most of existing conflict detection and resolution algorithms can be categorized into the deterministic and probabilistic approaches [5]. For the probabilistic conflict detection in the presence

of uncertainty, the empirical distribution model of future aircraft positions [6, 7, 8], the dynamical model by using stochastic differential equations [9, 10] and the probabilistic aircraft model based on the hybrid systems [11, 12] are used to describe the aircraft motion. Using the probabilistic aircraft motion model, the conflict probability between aircraft is estimated to detect a possible conflict. In addition, the conflict resolution problem is often formulated as an optimal control problem to determine the optimal conflict resolution trajectory. The stochastic optimal control problem is solved to generate the optimal conflict-free trajectory in the presence of uncertainty. In the previous works, Monte Carlo simulation [9], a Markov chain Monte Carlo framework [13] and Bayesian optimal design [14] are applied to determine an optimal control input, and the stochastic optimal control problem is solved by a Markov chain approximation and the Jacobi iteration [15].

In this study, a near-optimal conflict-free trajectory generation algorithm is proposed to determine the conflict resolution trajectory under wind uncertainty in real time, whereas most of the existing probabilistic conflict resolution methods mentioned above require much computation time and are difficult to implement in the real applications of ATM system. As to the uncertainty during flight, the wind prediction error, especially the spatially correlated wind error [10, 11, 16], is considered because the wind correlation may have a significant effect on the aircraft motion and therefore conflict detection and resolution [11]. In addition, we propose novel probabilistic conflict detection and resolution algorithms by employing the generalized polynomial chaos (gPC) method [17, 18, 19], which can determine the evolution of uncertainty in the complex nonlinear dynamical systems with high computational efficiency. To detect potential conflicts, the conflict probability between aircraft is estimated by the probabilistic conflict detection algorithm. For the conflict resolution problem, we apply the pseudospectral method [20] which is a recently developed numerical method to solve deterministic nonlinear optimal control problems. A numerical algorithm incorporating

the gPC method into the pseudospectral method is proposed to deal with stochastic elements and solve the stochastic optimal control problems. The stochastic optimal control method is combined with the probabilistic conflict detection algorithm to guarantee the resolution of potential conflicts between aircraft under the wind uncertainty. Moreover, inspired by a spatial statistical approach for synthesizing near-optimal feedback controllers [21], response surface methodology for generating optimal conflict-free trajectories is proposed by using the gPC algorithm, especially the recently developed gPC algorithm based on convex optimization [22, 23], which is a powerful numerical approach for the stochastic models with a large number of random variables. By constructing the response surfaces, the near-optimal conflict-free trajectories starting from any given initial states under the wind uncertainty are generated in real time without actually solving the stochastic optimization problems and sacrificing accuracy.

The paper is organized as follows. Section 2 presents the probabilistic conflict detection and resolution algorithms employing the gPC method. In section 3, response surface methodology is introduced to generate near-optimal conflict-free trajectories in real time. In section 4, the conflict detection and resolution problem among multiple aircraft is formulated and solved. In addition, the response surfaces of the optimal conflict-free trajectories are constructed, and the near-optimal conflict-free trajectories starting from any given initial states are generated. Through numerical simulations, the effectiveness and performance of the proposed stochastic algorithms are evaluated and demonstrated. Finally, conclusions and future research directions are provided in section 5.

2 Probabilistic Conflict Detection and Resolution

In this section, we first introduce the stochastic aircraft dynamics including spatially correlated wind errors, and propose a conflict detection algorithm based on the gPC method. After that, the stochastic optimal control method incorpo-

rating the gPC algorithm into the pseudospectral method is developed to solve the conflict resolution problem.

2.1 Stochastic Aircraft Dynamics

We consider the conflicts between aircraft in two-dimensional horizontal plane in which the aircraft coming from different directions merge to the waypoint. The aircraft dynamics are given by the following point mass model with three state variables $\boldsymbol{x} = (x, y, \psi)^T$ and one control variable u:

$$\dot{x} = v\cos\psi + w_x, \qquad (1)$$
$$\dot{y} = v\sin\psi + w_y, \qquad (2)$$
$$\dot{\psi} = u, \qquad (3)$$

where x and y are the Cartesian coordinates; ψ is the heading angle; v is the true airspeed and assumed to be constant; and w_x and w_y are the stochastic wind velocities in the x and y directions, respectively.

As to the wind uncertainty, the wind model contains the deterministic and stochastic components. In this study, the deterministic component representing the meteorological prediction is ignored and set to zero for simplicity. The wind model accounts for only the stochastic component, i.e., the wind prediction error representing the uncertainty in the deterministic meteorological prediction. Thus, the wind velocities w_x and w_y are referred to the wind prediction errors. In this study, to describe the wind errors more realistically, the spatially correlated wind model is considered. On the basis of the correlated wind model [11, 16], $w_x(x, y)$ and $w_y(x, y)$ are assumed to be Gaussian random processes with zero mean and the following exponential covariance function:

$$
\begin{aligned}
C\left((x,y),(x',y')\right) = \\
\sigma_w^2 \exp\left(-\mu_x|x-x'|\right)\exp\left(-\mu_y|y-y'|\right), (4)
\end{aligned}
$$

where σ_w is the standard deviation of the wind error and set to 10.40 kt [24]; and the parameters μ_x and μ_y are set to the same value of $1/182$ [11, 16]. As the distance difference increases, the correlation described in Eq. (4) decays exponentially. The random processes $w_x(x, y)$ and $w_y(x, y)$ are approximated as a linear combination of deterministic functions multiplied by independent random variables using the Karhunen-Loeve (KL) expansion [10, 25]:

$$w_x(x,y) \approx \sum_{i=1}^{N_{\mathrm{KL}}}\left(\sqrt{\lambda_i}g_i(x,y)\theta_{xi}\right), \qquad (5)$$

$$w_y(x,y) \approx \sum_{i=1}^{N_{\mathrm{KL}}}\left(\sqrt{\lambda_i}g_i(x,y)\theta_{yi}\right), \qquad (6)$$

where θ_{xi} and θ_{yi} are the independent standard Gaussian random variables; N_{KL} is the number of independent random variables; and λ_i and $g_i(x,y)$ are the eigenvalue and eigenfunction of the following integral equation in descending order of the magnitude of the eigenvalue λ_i, respectively:

$$\lambda_i g_i(x,y) = \int_D C\left((x,y),(x',y')\right)g_i(x',y')dx'dy',$$

where x and y are defined over a given domain D. Thus, the wind error is represented as the spatially correlated wind error with the finite number of independent random variables by using the KL expansion. (See, e.g., Ref. [25] for more detailed discussions.)

A conflict is defined as a situation where two or more aircraft experience a loss of the minimum separation established by ICAO [26]. Computing the distance between each pair of aircraft, we can identify the potential conflicts. To avoid the conflict, the two aircraft i and j need to satisfy the following safety constraint:

$$
\begin{aligned}
d_{H\min} \leq L_{ij} = \sqrt{(x_i - x_j)^2 + (y_i - y_j)^2} \\
(\forall i,j \in \{1,\ldots,s\} : i \neq j), \qquad (7)
\end{aligned}
$$

where the subscript i and j denote the ith and jth aircraft; s is the total number of aircraft; $d_{H\min}$ is the horizontal separation requirement; and $L_{ij}(= L_{ji})$ is the horizontal distance between the ith and jth aircraft. The aircraft positions x and y in Eq. (7) become the random variables because Eqs. (1) and (2) contain the stochastic terms w_x and w_y. Since x and y are the random variables, the horizontal distance between aircraft L given

by Eq. (7) also becomes a random variable. L cannot be determined analytically, and it needs to be calculated numerically. In this study, we propose the novel conflict detection algorithm based on the computationally efficient gPC method to calculate L. To detect possible conflicts, L is computed by the gPC algorithm, which will be described in more detail in section 2.2, and therefore the conflict probability between aircraft can be estimated as described in section 2.3.

2.2 Generalized Polynomial Chaos

One of the most commonly used methods to determine the evolution of uncertainty in dynamical systems is the Monte Carlo (MC) method. The MC method generates random sample points of random variables based on their prescribed probability density functions. Each random sample point is inserted into the stochastic model, and the stochastic problem is transformed into the deterministic problem that can be solved by using a deterministic solver. The statistical information (e.g., expected value, variance and covariance) can be calculated by using an ensemble of deterministic solutions. The MC method is straightforward to implement because it only requires the repetitive application of a deterministic solver. However, it is well known that the mean converges slowly and a large number of sample points is needed for accurate results, which implies excessive computational cost.

The gPC method [17, 18, 19] can reduce the computational effort significantly by approximating a stochastic solution as expansions of independent random variables using orthogonal polynomials. By using the gPC method, the stochastic solution $z(\boldsymbol{\theta})$ is approximated by the summation of the orthogonal polynomials of the independent random variables $\boldsymbol{\theta} = (\theta_1, \ldots, \theta_N) \in \mathbb{R}^N$, where N is the number of random variables. The Pth order approximation of the stochastic solution $z_P(\boldsymbol{\theta})$ is written as the following equation:

$$z_P(\boldsymbol{\theta}) = \sum_{m=1}^{M} C_m \Phi_m(\boldsymbol{\theta}) = \boldsymbol{\Phi}(\boldsymbol{\theta})\boldsymbol{C}, \quad (8)$$

$$\Phi_m(\boldsymbol{\theta}) = \prod_{i=1}^{N} \phi_i^{(l_i)}(\theta_i), \quad (9)$$

where $\boldsymbol{C}$ is the vector of the expansion coefficient C_m ($m = 1, \ldots, M$) defined as $\boldsymbol{C} = (C_1, \ldots, C_M)^T$; and $\boldsymbol{\Phi}(\boldsymbol{\theta})$ is the vector of the multivariate orthogonal polynomial basis function $\Phi_m(\boldsymbol{\theta})$ defined as $\boldsymbol{\Phi}(\boldsymbol{\theta}) = (\Phi_1(\boldsymbol{\theta}), \ldots, \Phi_M(\boldsymbol{\theta}))$. $\Phi_m(\boldsymbol{\theta})$ is obtained from the l_ith order one-dimensional polynomial basis function $\phi_i^{(l_i)}(\theta_i)$ of each random variable θ_i by the tensor product rule described in Eq. (9). l_i satisfies the following condition: $p_m = \sum_{i=1}^{N} l_i \leq P$, where p_m ($m = 1, \ldots, M$) is the sum of the order of the one-dimensional polynomial of the ith random variable $\phi_i^{(l_i)}(\theta_i)$ in Eq. (9); and P is the approximation order of the stochastic solution and the maximum degree of the multivariate polynomial Φ_m. M is the total number of tensor product basis functions and determined by the binomial coefficient: $M = \binom{N+P}{N}$. In addition, the normalized orthogonal (orthonormal) polynomial is used by satisfying the following orthogonality condition: $E[\phi_i^{(j)}(\theta_i)\phi_i^{(k)}(\theta_i)] = \int \phi_i^{(j)}(\theta_i)\phi_i^{(k)}(\theta_i)\rho_i(\theta_i)d\theta_i = \delta_{jk}$, where $E[\cdot]$ denotes the expectation operator; δ_{jk} is the Kronecker delta function; and $\rho_i(\theta_i)$ is the probability density function corresponding to the ith random variable θ_i. The best choice of the orthonormal polynomials depends on the type of $\rho_i(\theta_i)$ to achieve better convergence [17]. For example, Hermite polynomials are used with the Gaussian random variables. (See Ref. [17] for more detailed discussions.) In this study, the Gaussian random variables are considered in Eqs. (5) and (6), and Hermite polynomials are used. Since $\Phi_m(\boldsymbol{\theta})$ is the orthonormal polynomial, C_m in Eq. (8) is determined by the following equation:

$$C_m = E[z(\boldsymbol{\theta})\Phi_m(\boldsymbol{\theta})] = \int z(\boldsymbol{\theta})\Phi_m(\boldsymbol{\theta})\rho(\boldsymbol{\theta})d\boldsymbol{\theta}, \quad (10)$$

where $\rho(\boldsymbol{\theta})$ is the joint probability density function: $\rho(\boldsymbol{\theta}) = \prod_{i=1}^{N} \rho_i(\theta_i)$.

There are two main methods to determine C_m, i.e., the Galerkin and stochastic collocation methods [17, 18, 19]. With respect to implementation, a disadvantage of the Galerkin method is that it can be cumbersome and difficult to implement for complex nonlinear systems [19]. In contrast, the stochastic collocation approach is straightforward to implement because it uses the

strategically selected sample points, i.e., collocation points, of the random variables and repetitive executions of deterministic simulations as in the MC method. However, unlike the MC method, the stochastic solution is expressed as the orthonormal polynomials of the random variables with a significantly small number of collocation points. Therefore, the stochastic collocation form of the gPC method is employed to determine C_m.

Applying the stochastic collocation method, the integral in Eq. (10) can be approximated by using the Gaussian quadrature. A set of collocation points and quadrature weights is chosen on the basis of the quadrature rule. The q-point univariate quadrature operator $\mathcal{U}^q$ approximates the polynomial $\phi(\theta)$ by using the set of q collocation points $\theta^{(j)}$ and associated weights $\alpha^{(j)}$ ($j = 1,\ldots,q$): $\mathcal{U}^q[\phi(\theta)] = \sum_{j=1}^{q} \phi(\theta^{(j)})\alpha^{(j)} \approx \int_{-\infty}^{\infty} \phi(\theta)\rho(\theta)d\theta$. The quadrature weight $\alpha^{(j)}$ satisfies the following condition: $\sum_{j=1}^{q} \alpha^{(j)} = 1$. As q gets larger, the accuracy of the quadrature can be increased. In addition, the N-dimensional quadrature is readily derived from the one-dimensional quadrature by the tensor product rule. The N-dimensional tensor grid quadrature operator $\mathcal{T}$ is extended from the q-point univariate quadrature $\mathcal{U}^q$: $\mathcal{T}^{q,N} = \mathcal{U}_1^q \otimes \cdots \otimes \mathcal{U}_N^q$. The total number of collocation points is q^N determined by the tensor product rule. In general, as the number of random variables N gets larger, the tensor grid $\mathcal{T}$ suffers the *curse of dimensionality*. Thus, in this study, we employ the sparse grid quadrature based on the Smolyak rule [27, 28]. The sparse grid with Q collocation points $\theta^{(j)}$ and associated weights $\alpha^{(j)}$ ($j = 1,\ldots,Q$) consists of a much smaller number of collocation points than that of the tensor grid, and it can reduce the computational cost and increase the number of random variables. To reduce the number of collocation points, the Smolyak approach uses a strategically chosen linear combination of the tensor grid while retaining the accuracy of the quadrature. On the basis of the Smolyak rule, the N-dimensional sparse grid quadrature operator $\mathcal{S}$ is derived from the q-point one-dimensional quadrature $\mathcal{U}^q$:

$$S^{l,N} = \sum_{N+1 \leq |\boldsymbol{q}| \leq l+N} (-1)^{l+N-|\boldsymbol{q}|} \binom{N-1}{l+N-|\boldsymbol{q}|} (\mathcal{U}^{q_1} \otimes \cdots \otimes \mathcal{U}^{q_N}), \quad (11)$$

where l is the accuracy level of the sparse grid; and $|\boldsymbol{q}| = \sum_{i=1}^{N} q_i$ is the multi-index. As l gets larger, the accuracy of the sparse grid quadrature can be increased. The accuracy level l and the dimension N determine the number of collocation points Q in the sparse grid quadrature. As in the MC method, the stochastic problem is transformed into the deterministic problem on each collocation point and can be solved by repetitive application of a deterministic solver.

By using the stochastic collocation method based on the sparse grid quadrature rule described in Eq. (11), the approximation of C_m in Eq. (10) is given by the following equation:

$$C_m \approx \sum_{j=1}^{Q} z(\boldsymbol{\theta}^{(j)})\Phi_m(\boldsymbol{\theta}^{(j)})\alpha^{(j)}, \quad (12)$$

where $z(\boldsymbol{\theta}^{(j)})$ denotes the deterministic solution by using the jth collocation point $\boldsymbol{\theta}^{(j)}$. Thus, the approximate stochastic solution $z_P(\boldsymbol{\theta})$ is determined by Eqs. (8) and (12) as the orthonormal polynomials of the random variables $\boldsymbol{\theta}$. As described in Eqs. (8) and (12), $z_P(\boldsymbol{\theta})$ is the distribution function of $\boldsymbol{\theta}$ and can be evaluated for any given random inputs. In addition, the statistical information (expected value and variance) of $z_P(\boldsymbol{\theta})$ can be calculated by using C_m given by Eq. (12). The expected value and variance of $z_P(\boldsymbol{\theta})$ are described as the following equations:

$$E[z_P(\boldsymbol{\theta})] = \int \left[\sum_{m=1}^{M} C_m \Phi_m(\boldsymbol{\theta}) \right] \rho(\boldsymbol{\theta})d\boldsymbol{\theta},$$
$$= C_1, \quad (13)$$

$$Var[z_P(\boldsymbol{\theta})] = E[(z_P(\boldsymbol{\theta}) - E[z_P(\boldsymbol{\theta})])^2],$$
$$= \int \left[\sum_{m=1}^{M} C_m \Phi_m(\boldsymbol{\theta}) - C_1 \right]^2 \rho(\boldsymbol{\theta})d\boldsymbol{\theta},$$
$$= \sum_{m=2}^{M} [C_m]^2, \quad (14)$$

where $Var[\cdot]$ denotes the variance operator.

The procedures to determine the stochastic solution $z(\boldsymbol{\theta})$ and its statistical information are listed as follows:

1. Generate a set of Q collocation points of random variables $\boldsymbol{\theta}^{(j)}$ and associated weights $\alpha^{(j)}$ $(j = 1, \ldots, Q)$ based on the sparse grid quadrature in Eq. (11).

2. Calculate the value of the orthonormal polynomial $\Phi_m(\boldsymbol{\theta}^{(j)})$ on each collocation point $\boldsymbol{\theta}^{(j)}$ $(j = 1, \ldots, Q,\ m = 1, \ldots, M)$ by Eq. (9).

3. Determine the deterministic solution $z(\boldsymbol{\theta}^{(j)})$ on each collocation point $\boldsymbol{\theta}^{(j)}$ $(j = 1, \ldots, Q)$.

4. Compute the coefficient C_m $(m = 1, \ldots, M)$ in Eq. (12).

5. Determine the approximate stochastic solution $z_P(\boldsymbol{\theta})$ in Eq. (8).

6. Calculate the statistical information of the approximate stochastic solution $z_P(\boldsymbol{\theta})$, the expected value $E[z_P(\boldsymbol{\theta})]$ in Eq. (13) and the variance $Var[z_P(\boldsymbol{\theta})]$ in Eq. (14), by using C_m.

2.3 Conflict Probability Estimation for Conflict Detection

To detect potential conflicts between aircraft, we need to compute the distance between each pair of aircraft. Since the wind errors in Eqs. (5) and (6) are described by the random variables, the horizontal distance between aircraft L in Eq. (7) is also the random variable. By using the gPC method mentioned in section 2.2, L can be solved, and the statistical information of L ($E[L]$ and $Var[L]$) is calculated. The probability density function of L, $\rho(L)$, is unknown; however, the probability distribution of a random variable can be characterized by its moments, and the unknown distribution can be estimated by the moment matching technique. Using the statistical information of L, $\rho(L)$ is approximated by

the one-dimensional truncated Gaussian distribution by matching the first two moments: $L \sim \mathcal{N}(E[L], Var[L])$ $(L \geq 0)$. Accordingly, on the basis of the safety constraint in Eq. (7), the conflict probability between the ith and jth aircraft $\Pr\left[\mathcal{C}_{ij}\right]$ is given by the following equation:

$$\Pr\left[\mathcal{C}_{ij}\right] = \Pr\left[L_{ij} \leq d_{H\min}\right] = \int_0^{d_{H\min}} \rho(L_{ij}) dL_{ij}, \tag{15}$$

where $\Pr[\cdot]$ denotes the probability of an event; and $\mathcal{C}_{ij}$ indicates conflict between the ith and jth aircraft.

The procedures to estimate the conflict probability between the ith and jth aircraft are listed as follows.

1. Calculate the statistical information of the distance between aircraft L_{ij} ($E(L_{ij})$ and $Var(L_{ij})$) by using the gPC method described in section 2.2.

2. Determine the probability density function of L_{ij}, $\rho(L_{ij})$.

3. Estimate the conflict probability between aircraft $\Pr\left[\mathcal{C}_{ij}\right]$ in Eq. (15).

Using the probabilistic conflict detection algorithm mentioned above, the potential conflicts can be detected. For the resolution of the potential conflicts, the stochastic optimal control method is proposed to determine the conflict-free trajectory under the wind uncertainty in section 2.4.

2.4 Stochastic Optimal Control

The following continuous-time stochastic optimal control problem is considered. Determine the state variables $\boldsymbol{x}(t)$, the control variables $\boldsymbol{u}(t)$ and the terminal time t_f on the time interval $t \in [0, t_f]$ that minimize the cost function:

$$J = E\left[g_M(\boldsymbol{x}(0), \boldsymbol{x}(t_f)) + \int_0^{t_f} g_L(\boldsymbol{x}(t), \boldsymbol{u}(t), t) dt\right], \tag{16}$$

subject to the dynamic constraints:

$$\dot{\boldsymbol{x}}(t) = \boldsymbol{f}(\boldsymbol{x}(t), \boldsymbol{u}(t), t), \tag{17}$$

the boundary conditions:

$$\boldsymbol{b}_{\min} \leq E\left[\boldsymbol{b}(\boldsymbol{x}(0),\boldsymbol{x}(t_f))\right] \leq \boldsymbol{b}_{\max}, \qquad (18)$$

and the chance constraints [29, 30]:

$$\boldsymbol{\eta}_{\min} \leq \Pr\left[\boldsymbol{c}_{\min} \leq \boldsymbol{c}(\boldsymbol{x}(t),\boldsymbol{u}(t),t) \leq \boldsymbol{c}_{\max}\right] \leq \boldsymbol{\eta}_{\max}, \qquad (19)$$

where g_M and g_L define the Mayer and Lagrange terms in the cost function, respectively; $\boldsymbol{f}$ is the system dynamics; $\boldsymbol{b}$ expresses the boundary condition functions; $\boldsymbol{c}$ defines the path constraint functions; and $\boldsymbol{\eta}$ is the confidence level. The chance constraints are formulated by the previous studies [29, 30], which can restrict the probability of conflict to a given range. In this study, we formulate the conflict probability as the chance constraints given by Eq. (19).

In this study, we apply the direct collocation pseudospectral method [20], which is the recently developed numerical method to solve deterministic nonlinear optimal control problems. In the pseudospectral method, the time-dependent dynamic variables are approximated and parameterized using polynomials, and the cost function and the constrains are also discretized using a quadrature rule. Thus, the continuous-time optimal control problem is discretized and transcribed into the nonlinear programming (NLP) problem. Then, an NLP solver such as sequential quadratic programming (SQP) is applied to determine the optimal solution. In this study, we employ the General Pseudospectral Optimization Software (GPOPS) [31], which is performed in MATLAB and using SNOPT [32] as the NLP solver. By using GPOPS, the continuous-time optimal control problem is transformed into the NLP problem for the SNOPT NLP solver which finds the optimal solution. To deal with the stochastic elements and solve the stochastic optimal control problem (Eqs. (16)–(19)), the stochastic solution including the statistical information is approximated by the theory of the gPC method mentioned in section 2.2. Therefore, by incorporating the gPC algorithm into the pseudospectral method, we can solve the stochastic optimal control problem.

To solve the conflict resolution problem, the stochastic optimal control method is combined with the proposed probabilistic conflict detection algorithm to guarantee the resolution of potential conflicts between aircraft under the wind uncertainty. By solving the stochastic optimal control problem for conflict resolution, the optimal conflict-free trajectory under the wind uncertainty is generated.

3 Near-Optimal Conflict-Free Trajectory Generation

By using the stochastic optimal control method mentioned in section 2.4, we can generate the optimal conflict-free trajectory starting from an given initial point. However, the initial states on the precomputed optimal trajectory may differ from the actual initial states because of the uncertainty during flight, and another optimal control problem starting from the different actual initial states is necessary to be solved to obtain the correct optimal trajectory. Therefore, in this study, we introduce an efficient numerical algorithm for generating near-optimal solutions in real time by constructing response surface models or surrogate models based on the gPC algorithm. By constructing the response surfaces of the optimal conflict-free trajectories under the wind uncertainty, the approximate optimal conflict-free trajectories from any given initial states can be obtained quickly without actually solving the stochastic optimal control problems.

Response surface models or surrogate models approximate the input-output behavior of an original simulation, and an output can be obtained from a certain input without actually executing the simulation. In this study, the response surfaces based on the gPC algorithm are constructed for generating near-optimal conflict-free trajectories. The inputs of the response surfaces are the initial states $\boldsymbol{x}_0$, and the outputs are the states $\boldsymbol{x}^*$, controls $\boldsymbol{u}^*$ and terminal time $\boldsymbol{t}_f^*$ of the optimal conflict-free trajectory. By the theory of the gPC method, the stochastic solution can be approximated by the polynomials of the independent random variables as described in Eq. (8). $\boldsymbol{x}_0$ are assumed to be the random variables, and $\boldsymbol{x}^*$, $\boldsymbol{u}^*$ and $\boldsymbol{t}_f^*$ are approximated as the functions of

x_0 in Eq. (8). Thus, by using the gPC method, the Pth order approximations of the optimal solutions $x_P^*(x_0)$, $u_P^*(x_0)$ and $t_{fP}^*(x_0)$ represent the response surfaces of the optimal conflict-free trajectories (inputs: initial states x_0, outputs: approximate optimal states x_P^*, controls u_P^* and terminal time t_{fP}^* of conflict-free trajectory).

Using the stochastic collocation method mentioned in section 2.2, the expansion coefficients C in Eq. (8) are determined by using the solutions on the Q collocation points of the initial states $x_0^{(j)}$ ($j = 1, \ldots, Q$), i.e., the optimal states $x^*(x_0^{(j)})$, controls $u^*(x_0^{(j)})$ and terminal time $t_f^*(x_0^{(j)})$ of the conflict-free trajectory starting from the jth collocation point of the initial states $x_0^{(j)}$ ($j = 1, \ldots, Q$). Accordingly, Q stochastic optimal control problems are needed to be solved for constructing the response surfaces. The stochastic collocation method is computationally efficient when the number of random variables is small. However, unlike the wind errors in section 2, the number of random variables or inputs of the response surfaces becomes large. As the number of random variables increases, the number of collocation points is considerably larger even though the sparse grid is used. Therefore, to reduce the computational cost for constructing the response surfaces, we introduce the recently developed gPC algorithm based on convex optimization [22, 23] to determine the coefficients C, which is similar approach to the stochastic collocation method but requires a much smaller number of sample points than the stochastic collocation method.

To compute C, the following convex optimization problem is solved:

$$\underset{C \in \mathbb{R}^M}{\text{minimize}} \quad \|WC\|_1 + \beta\|\tilde{\Lambda}(\tilde{z} - \tilde{\Phi}C)\|_2. \quad (20)$$

$\|\cdot\|_1$ and $\|\cdot\|_2$ denote the l_1 and l_2 norms, respectively. $\tilde{z}$ is the vector of the solutions on the Q sample points $\theta^{(j)}$ ($j = 1, \ldots, Q$): $\tilde{z} = (z(\theta^{(1)}), \ldots, z(\theta^{(Q)}))^T$. $\tilde{\Phi}$ is the matrix of the

multivariate polynomials given by Eq. (9):

$$\tilde{\Phi} = \begin{pmatrix} \Phi(\theta^{(1)}) \\ \vdots \\ \Phi(\theta^{(Q)}) \end{pmatrix},$$

$$= \begin{pmatrix} \Phi_1(\theta^{(1)}), & \cdots & ,\Phi_M(\theta^{(1)}) \\ \vdots & \ddots & \vdots \\ \Phi_1(\theta^{(Q)}), & \cdots & ,\Phi_M(\theta^{(Q)})) \end{pmatrix}.$$

W is the diagonal weighting matrix and β is the scalar weight. W is defined as $W = \text{diag}(W(p_m)) \in \mathbb{R}^{M \times M}$, where p_m is the order of Φ_m and $p_m \leq P$, and $W(p_m)$ ($m = 1, \ldots, M$) is the scalar weight determined by the following properties:

$$W(p_m) > 0,$$
$$W(p_m) > W(p_l) \quad \text{if} \quad p_m > p_l,$$
$$\max_m W(p_m) = 1 \quad (\forall l, m \in \{1, \ldots, M\} : l \neq m).$$

$\tilde{\Lambda}$ is the diagonal matrix defined as $\tilde{\Lambda} = \text{diag}(\tilde{\lambda})$, where $\tilde{\lambda}$ is the vector of the values of the joint probability density function $\rho(\theta)$ at the sample points $\theta^{(j)}$ ($j = 1, \ldots, Q$): $\tilde{\lambda} = (\rho(\theta^{(1)}), \ldots, \rho(\theta^{(Q)}))^T$. Unlike the stochastic collocation method, the sample point $\theta^{(j)}$ ($j = 1, \ldots, Q$) is randomly selected as in the MC method. The number of sample points Q is determined by considering the convergence of the ∞ norm of the difference between two subsequent coefficients vectors $\|C^{*(Q+1)} - C^{*(Q)}\|_\infty$, where $C^{*(Q)}$ denotes the optimized coefficients obtained by using Q sample points and solving the convex optimization problem in Eq. (20). (See Ref. [22] for more detailed discussions.)

By solving the convex optimization problem in Eq. (20), the coefficients C are determined, and the stochastic solution z_P in Eq. (8) is computed. In this study, we employ CVX, a package for specifying and solving convex programs [33, 34] to solve the convex optimization problem in Eq. (20). Therefore, the response surfaces of the optimal conflict-free trajectories $x_P^*(x_0)$, $u_P^*(x_0)$ and $t_{fP}^*(x_0)$ (inputs: initial states x_0, outputs: approximate optimal states x_P^*, controls u_P^* and terminal time t_{fP}^* of conflict-free trajectory)

are constructed by solving the Q stochastic optimal control problems and the convex optimization problem in Eq. (20). The optimal conflict-free trajectories starting from any given initial states under the wind uncertainty can be generated from the response surfaces in real time without actually solving the stochastic optimal control problem.

Finally, the procedures to generate the near-optimal conflict-free trajectory by constructing the response surfaces are listed as follows:

1. Generate Q sample points of initial states $\boldsymbol{x}_0^{(j)}$ $(j = 1, \ldots, Q)$ randomly.

2. Calculate the values of the orthogonal polynomial basis functions $\Phi_m(\boldsymbol{x}_0^{(j)})$ $(j = 1, \ldots, Q, \ m = 1, \ldots, M)$ by using Eq. (9).

3. Determine the optimal states $\boldsymbol{x}^*(\boldsymbol{x}_0^{(j)})$, controls $\boldsymbol{u}^*(\boldsymbol{x}_0^{(j)})$ and terminal time $\boldsymbol{t}_f^*(\boldsymbol{x}_0^{(j)})$ of the conflict-free trajectory starting from each sample point of the initial states $\boldsymbol{x}_0^{(j)}$ $(j = 1, \ldots, Q)$ by using the stochastic optimal control method mentioned in section 2.4. (Solve Q stochastic optimal control problems.)

4. Solve the convex optimization problem in Eq. (20) to determine the coefficients $\boldsymbol{C}$ in Eq. (8).

5. Determine the Pth order approximations of the optimal conflict-free trajectories in Eq. (8), and construct the response surfaces of the optimal conflict-free trajectories $\boldsymbol{x}_P^*(\boldsymbol{x}_0)$, $\boldsymbol{u}_P^*(\boldsymbol{x}_0)$ and $\boldsymbol{t}_{fP}^*(\boldsymbol{x}_0)$ (inputs: initial states $\boldsymbol{x}_0$, outputs: approximate optimal states $\boldsymbol{x}_P^*$, controls $\boldsymbol{u}_P^*$ and terminal time $\boldsymbol{t}_{fP}^*$ of conflict-free trajectory).

6. Generate the near-optimal states $\boldsymbol{x}_P^*(\boldsymbol{x}_0)$, controls $\boldsymbol{u}_P^*(\boldsymbol{x}_0)$ and terminal time $\boldsymbol{t}_{fP}^*(\boldsymbol{x}_0)$ of the conflict-free trajectory by using the response surfaces with any given inputs of the initial states $\boldsymbol{x}_0$.
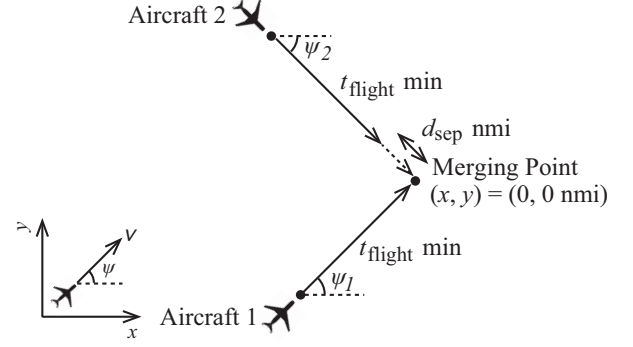

Fig. 1 Conflict scenario for conflict detection problem.

4 Numerical Simulations

In this section, to demonstrate the performance and effectiveness of the proposed stochastic algorithms, numerical simulations of the two-dimensional conflict detection and resolution problem among multiple aircraft are conducted. First, the conflict detection problem is solved by the probabilistic conflict detection algorithm based on the gPC method. After that, the conflict resolution problem among multiple aircraft is considered by the stochastic optimal control method. Finally, the near-optimal conflict-free trajectory generation problem is formulated and solved. The simulations are performed on a computer with a 2.3 GHz Intel Core i5-2410M processor and 4 GB RAM.

4.1 Probabilistic Conflict Detection

4.1.1 Conflict Detection Problem

As shown in Fig. 1, we consider the two-dimensional conflict scenario between the two aircraft, labeled 1 and 2. A conflict is defined by the minimum separation requirement $d_{H\min}$ established by ICAO [26], which is set to 5 nmi in en route airspace. As shown in Fig. 1, we consider the two aircraft flying toward the merging point $(x, y) = (0, 0 \text{ nmi})$ without any maneuvers or control inputs. The both aircraft fly level at the same altitude and the same constant airspeed v of 400 kt. The heading angle ψ_i $(i = 1, 2)$ $(-\pi/2 \leq \psi_i \leq \pi/2)$ is randomly set to a constant value: $\psi_1 = 0.49$ and $\psi_2 = -0.34$. In addition,
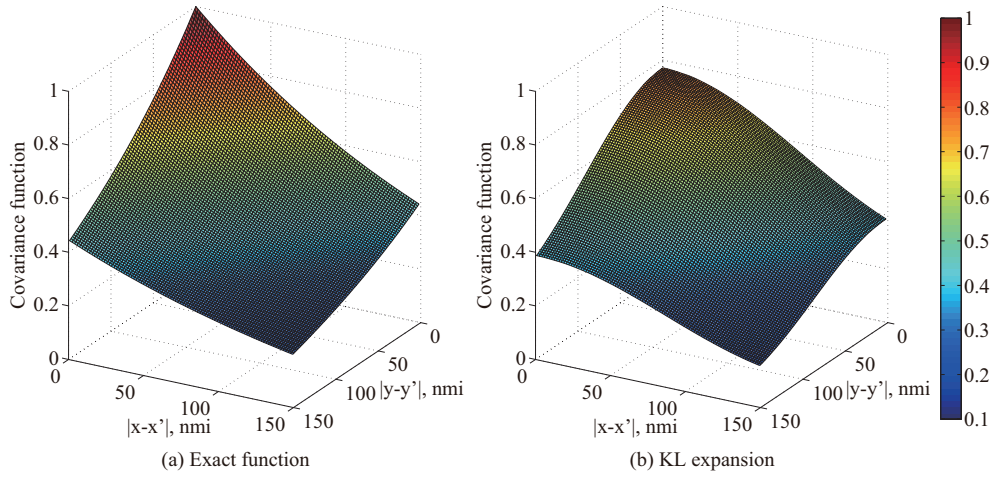
(a) Exact function   (b) KL expansion

Fig. 2 Comparison between exact covariance function and covariance function obtained with KL expansion.

as shown in Fig. 1, t_{flight} is the nominal flight time to the merging point for aircraft 1 in the absence of the wind field and set to 5 min. Aircraft 1 reaches the merging point in the absence of the wind field after t_{flight} min flight, and the nominal separation between aircraft 1 and 2 after t_{flight} min flight d_{sep} ($0 \le d_{\text{sep}} \le 5$ nmi) is randomly determined: $d_{\text{sep}} = 3.72$ nmi, as shown in Fig. 1. The initial positions are determined geometrically in the absence of the wind field.

As described in section 2.1, the spatially correlated wind model is considered by using the KL expansion. In Eqs. (5) and (6), the number of independent random variables N_{KL} is set to three, and the total number of random variables is six. To compute the KL expansion, x and y are defined over the domain D: $|x| \le 150$ nmi and $|y| \le 150$ nmi. Fig. 2 shows the comparison between the exact covariance function $C((x, y), (x', y'))$ in Eq. (4) and the covariance function $\tilde{C}((x, y), (x', y'))$ obtained with the KL expansion, where $\tilde{C}((x, y), (x', y')) = \sum_{i=1}^{N_{\text{KL}}} \lambda_i g_i(x, y) g_i(x', y')$. The root mean square (RMS) error between the exact covariance function and the covariance function obtained with the KL expansion is 0.036, which is small enough to suggest that the covariance function obtained with the KL expansion has good approximation accuracy. As N_{KL} gets larger, the covariance function can be obtained more accurately with the KL expansion. However, when the total number of random variables increases, the computa-

tional cost is considerably higher. Thus, in this study, N_{KL} is set to three, and the total number of random variables is six.

To demonstrate the effectiveness and performance of the conflict detection algorithm, the statistical information of the distance between aircraft L ($E[L]$ and $Var[L]$) is computed on the time interval $t \in [0, t_{\text{flight}}]$ by the gPC and MC methods, and the results are compared with each other.

4.1.2 Simulation Results of Conflict Detection Problem

The conflict detection problem mentioned in section 4.1.1 is solved by the probabilistic conflict detection algorithm, and the statistical information of the distance between aircraft L ($E[L]$ and $Var[L]$) is computed. Fig. 3 shows the normalized RMS errors in $E[L]$ and $Var[L]$ (at time instant $t = t_{\text{flight}} = 5$ min) computed by using the gPC and MC methods with different numbers of sample points. The circle marker on the blue line indicates the normalized RMS error obtained by conducting 100 runs of the MC simulation. The number of sample points is set to 10, 100, 1000, 10000 and 100000. The cross marker on the green line is the normalized RMS error by employing the gPC algorithm. For the gPC algorithm, the approximation order P is set to three, and the accuracy level l of the sparse grid is set to two to six. As l gets larger, the number of collocation points is increased: 13, 73, 257, 749 and 2021 ($l = 2$–6). To compute the normalized

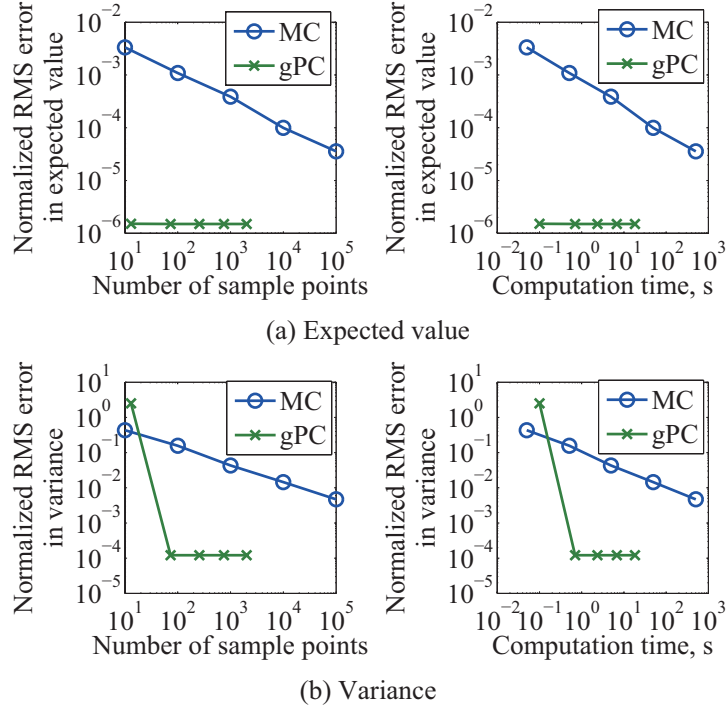(a) Expected value

(b) Variance

Fig. 3 Normalized root mean square (RMS) errors in expected value and variance of distance between aircraft.

RMS errors, the true values of $E[L]$ and $Var[L]$ are assumed to be the mean values obtained by conducting 100 runs of the MC simulation with 100000 sample points, and the RMS errors are normalized to the true values. The computation time (average time for each run) is proportional to the number of sample points in Fig. 3. As shown in Fig. 3, the gPC algorithm can estimate the accurate solution by using the much smaller number of sample points than the MC method. The MC method requires over 100000 sample points to yield the same accuracy as the gPC method. The computation time is correspondingly over 1000 s. On the other hand, the gPC algorithm requires only 73 collocation points (accuracy level $l = 3$) and approximately 0.5 s to obtain the reasonable approximate solution.

Therefore, the gPC method provides an accurate approximate solution while dramatically reducing computational cost. Using the MC method especially within the iterative process such as optimization process (e.g., optimal control problem for conflict resolution described in section 4.2) is computationally laborious and intractable, and our proposed computationally efficient algorithm can perform much faster than the
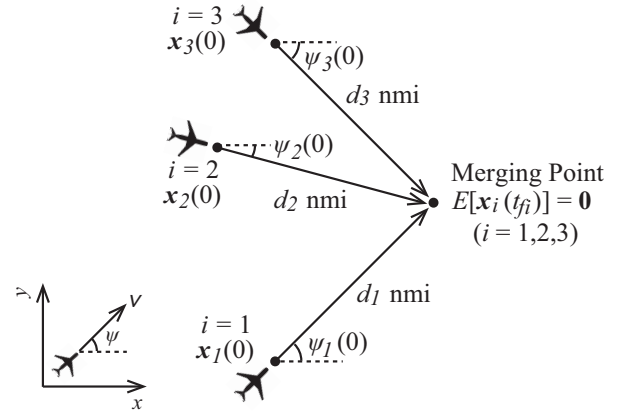

Fig. 4 Conflict scenario for conflict resolution problem.

MC method. Through the numerical simulations, the effectiveness and performance of the probabilistic conflict detection algorithm are demonstrated.

4.2 Stochastic Optimal Control for Conflict Resolution

4.2.1 Conflict Resolution Problem

We consider the conflict resolution problem among multiple aircraft in two-dimensional hor-
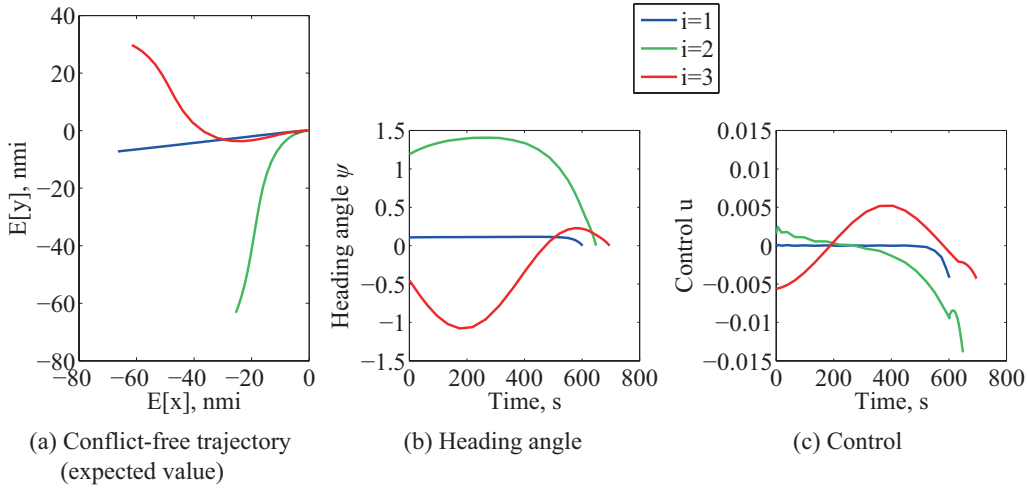
Fig. 5 Optimal conflict-free trajectory (expected value) and time histories of dynamic variables.

Table 1 Parameters for conflict resolution problem.

Parameters	Values
$(\psi_1(0), d_1 \text{ nmi})$	$(0.11, 66.88 \text{ nmi})$
$(\psi_2(0), d_2 \text{ nmi})$	$(1.19, 68.27 \text{ nmi})$
$(\psi_3(0), d_3 \text{ nmi})$	$(-0.45, 68.41 \text{ nmi})$

Table 2 Terminal time at merging point.

Parameters	Values, s
t_{f1}	601.97
t_{f2}	648.67
t_{f3}	695.81

izontal plane in which the aircraft coming from different directions merge to the waypoint. A conflict is defined by the required minimum separation standard established by ICAO [26], and the horizontal separation requirement $d_{H\min}$ is set to 5 nmi for the en route airspace. As shown in Fig. 4, we consider the conflict scenario among three aircraft. The merging point is set to $(x,y) = (0,0 \text{ nmi})$, and the initial condition $\boldsymbol{x}_i(0)$ ($i = 1,2,3$) is determined geometrically by the initial heading angle $\psi_i(0)$ ($-\pi/2 \leq \psi_i \leq \pi/2$) and the direct distance between the initial position and the merging point d_i ($65 \leq d_i \leq 70$ nmi):

$$\boldsymbol{x}_i(0) = (-d_i \cos \psi_i(0), -d_i \sin \psi_i(0), \psi_i(0))^T. \quad (21)$$

$\psi_i(0)$ and d_i are randomly determined, and the values of the parameters are shown in Table 1. We assume that the subscript i indicates the aircraft sequences of reaching the merging point in ascending order of the value i. Before solving the optimal control problem, the arrival sequences of the three aircraft are predetermined in ascending order of the magnitude of d_i ($i = 1,2,3$), where d_i is given by satisfying the following condition: $d_1 \leq d_2 \leq d_3$.

In addition, the terminal condition $\boldsymbol{x}_i(t_{fi})$ ($i = 1,2,3$) is given by:

$$E[\boldsymbol{x}_i(t_{fi})] = (0,0,0)^T, \quad (22)$$

where t_{fi} is the terminal time (time of arrival at the merging point, $t_{f1} \leq t_{f2} \leq t_{f3}$). Since $\boldsymbol{x}_i(t)$ contains the wind errors, the terminal condition in Eq. (22) is considered as the expected value. As to the wind uncertainty, the spatially correlated wind model is considered by using the KL expansion described in section 2.1. As in the numerical simulations of conflict detection in section 4.1, the number of independent random variables N_{KL} in Eqs. (5) and (6) is set to three, and the total number of random variables is six.

Furthermore, the aircraft dynamics are given by Eqs. (1)–(3), and the constraints on the variables are given as follows: $-\pi/2 \leq \psi \leq \pi/2$ and $-\pi/120 \leq u \leq \pi/120$. We consider the stochastic safety constraint condition that the required minimum conflict probability is 0.1 to yield the effective conflict resolution trajectory [6]:

$$\Pr\left[\mathcal{C}_{ij}\right] \leq 0.1 \quad (\forall i,j \in \{1,2,3\} : i \neq j), \quad (23)$$

where the conflict probability $\Pr\left[\mathcal{C}_{ij}\right]$ is given by
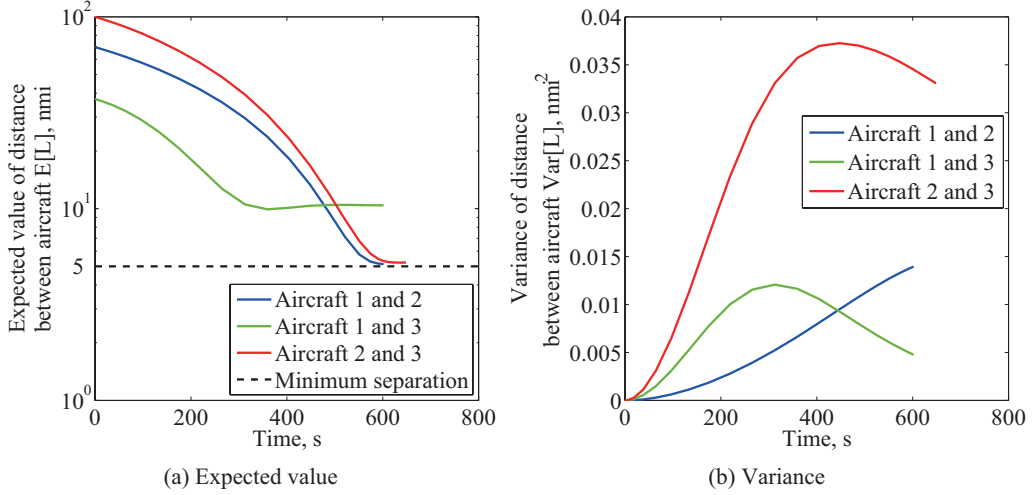
(a) Expected value

(b) Variance

Fig. 6 Time histories of expected values and variances of distances between aircraft.

Eq. (15). For solving the stochastic optimal control problem to determine the conflict-free trajectory, the following cost function J is minimized:

$$J = \sum_{i=1}^{3} \left(t_{fi} + 10^3 \int_0^{t_{fi}} |u_i(t)|^2 dt \right). \qquad (24)$$

As described in Eqs. (21)–(24), the multiple-phase (three-phase) optimal control problem is formulated: three aircraft ($i = 1, 2, 3$) and three conflicts ($\mathcal{C}_{12}, \mathcal{C}_{13}, \mathcal{C}_{23}$) are considered in the first phase ($t \in [0, t_{f1}]$); two aircraft ($i = 2, 3$) and one conflict ($\mathcal{C}_{23}$) are considered in the second phase ($t \in [t_{f1}, t_{f2}]$); and one aircraft ($i = 3$) is considered in the third phase ($t \in [t_{f2}, t_{f3}]$). Through the numerical simulations, the effectiveness and performance of the stochastic optimal control method are evaluated and demonstrated.

4.2.2 Simulation Results of Conflict Resolution Problem

We apply the proposed stochastic optimal control method to the conflict resolution problem described in section 4.2.1. For applying the gPC algorithm, on the basis of the numerical simulations of conflict detection in section 4.1.2, the approximation order P is set to three and the accuracy level l is set to three. Accordingly, the number of collocation points is 73 for six random variables.

By using the stochastic optimal control method based on the pseudospectral method, the

Table 3 Minimum distances between aircraft (expected values).

Pairs	Values, nmi
$\mathcal{C}_{12}$ (aircraft 1 and 2)	5.15
$\mathcal{C}_{13}$ (aircraft 1 and 3)	9.92
$\mathcal{C}_{23}$ (aircraft 2 and 3)	5.23

nonlinear optimal control problem can be solved, and the dynamic variables including the conflict resolution trajectory are optimized. Fig. 5 shows the expected value of the conflict resolution trajectory and the time histories of the state and control variables (except the aircraft position (x, y)). The blue, green and red lines indicate the solutions of aircraft 1, 2 and 3 ($i = 1$–3), respectively. Table 2 indicates the terminal time at the merging point for each aircraft. As shown in Fig. 5, aircraft 2 and 3 take a detour to avoid conflict, while aircraft 1 does not take a detour and flies toward the merging point without any conflict resolution maneuvers. It indicates that the trajectory of aircraft 1 is not affected by resolving conflict and these conflict resolution trajectories can minimize the cost function in Eq. (24).

In addition, Fig. 6 shows the time histories of the expected values $E[L]$ and variances $Var[L]$ of the distances between aircraft L, which are optimized to satisfy the stochastic safety constraint described in Eqs. (15) and (23). Since our proposed stochastic optimal control method incorporates the gPC algorithm, $E[L]$ and $Var[L]$ are

easily computed. As shown in Fig. 6, $Var[L]$ increases with time because the effect of the wind uncertainty accumulates over time, and the magnitude of $Var[L]$ indicates the effect of the wind uncertainty and correlation on the separation between aircraft. When the distance between aircraft is shorter, the wind errors between the two aircraft are highly correlated, and accordingly $Var[L]$ becomes smaller. Since the wind errors experienced by any two aircraft are correlated with each other, $Var[L]$ under the correlated wind error can be smaller than under the non-correlated wind error, which is the completely independent error on each aircraft. Moreover, Table 3 shows the minimum distances between aircraft in Fig. 6. The distances between aircraft L are optimized to satisfy the stochastic safety constraint described in Eqs. (15) and (23). By considering the stochastic safety constraint, the minimum distances between aircraft are larger than the minimum allowed separation of 5 nmi to guarantee the resolution of the potential conflicts. As shown in Table 3, the minimum distances have the margins from the minimum allowed separation of 5 nmi. It indicates that the conflict resolution trajectory can be guaranteed to avoid conflict under the wind uncertainty.

To generate the optimal conflict-free trajectory, the computation time for solving the conflict resolution problem is approximately 60 s by employing the computationally efficient gPC algorithm. According to the results of the conflict detection problem mentioned in section 4.1.2, it can be computationally intractable to use the MC method instead of the gPC algorithm. Our proposed stochastic optimal control method can optimize the dynamic variables including the conflict resolution trajectory efficiently, and the resolution of the potential conflicts is guaranteed by incorporating the conflict detection algorithm and considering the stochastic safety constraint described in Eqs. (15) and (23). Consequently, the stochastic optimal control method can provide the effective conflict resolution trajectory that can be guaranteed to avoid potential conflicts under the wind uncertainty. Through the numerical simulations, the effectiveness and performance of the stochastic optimal control method
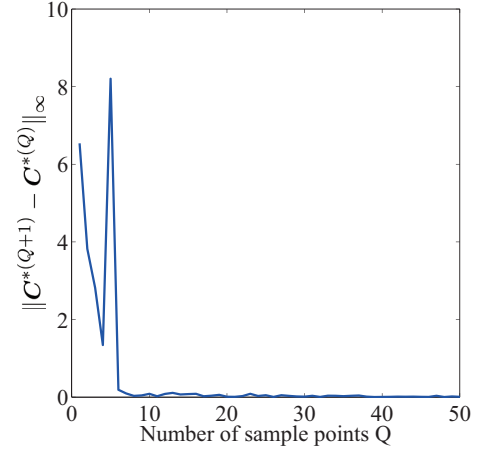

Fig. 7 Distance between two subsequent coefficients (coefficients for terminal time of aircraft 1 t_{f1}).

are evaluated and demonstrated.

4.3 Near-Optimal Conflict-Free Trajectory Generation

4.3.1 Problem Formulation of Near-Optimal Conflict-Free Trajectory Generation

On the basis of the problem formulation of stochastic optimal control for conflict resolution described in section 4.2.1, the near-optimal conflict-free trajectory generation problem is formulated to construct the response surfaces of the optimal conflict-free trajectories. As the inputs of the response surfaces, the random variables of the initial states are assumed to be Gaussian, and the means are consistent with the values of the initial conditions given by Eq. (21) and Table 1. The standard deviations of the initial x and y positions and heading angle ψ are set to 1 nmi and $\pi/36$, respectively. Since the conflict scenario among three aircraft is considered as shown in Fig. 4, the total number of random variables of the initial states or inputs of the response surfaces is nine.

To evaluate and demonstrate the effectiveness and performance of the response surface methodology, the response surfaces are constructed by using the two gPC algorithms based on convex optimization described in section 3 and the stochastic collocation method mentioned in section 2.2. For applying the gPC algorithm based on convex optimization, the approximation or-

Table 4 Maximum and root mean square (RMS) errors of states, controls and terminal time between near-optimal and optimal solutions (comparison between errors obtained by using gPC algorithms based on convex optimization and stochastic collocation method).

Parameters	Maximum errors[*]	RMS errors[*]	Maximum errors[†]	RMS errors[†]
x_1, nmi	0.032	0.0077	1.13	0.25
y_1, nmi	0.17	0.028	1.74	0.38
ψ_1	0.018	0.0036	0.20	0.055
x_2, nmi	1.01	0.39	3.45	0.89
y_2, nmi	0.69	0.29	2.63	0.66
ψ_2	0.19	0.064	0.30	0.77
x_3, nmi	0.27	0.064	1.12	0.33
y_3, nmi	0.36	0.11	1.17	0.27
ψ_3	0.043	0.0083	0.12	0.027
u_1	0.0012	0.00038	0.0081	0.0024
u_2	0.0085	0.0030	0.0104	0.0030
u_3	0.0015	0.00028	0.0043	0.00094
t_{f1}, s	0.48	0.16	9.90	2.28
t_{f2}, s	2.30	0.36	11.21	2.62
t_{f3}, s	2.32	0.36	11.23	2.53

[*] Response surfaces constructed by using gPC algorithm based on convex optimization

[†] Response surfaces constructed by using gPC algorithm based on stochastic collocation method

der P is set to three. To solve the convex optimization problem in Eq. (20), the weights $W(p_m)$ ($p_m = 0, 1, 2, 3$) are selected as $W(0) = 0.0001$ and $W(p_m) = p_m^2/9$ ($p_m = 1, 2, 3$), and the scalar weight β is set to 10^6. As we demonstrate in section 4.3.2, the number of sample points is set to 25, and therefore 25 optimal control problems starting from the different initial states are solved for constructing the response surfaces of the optimal conflict-free trajectories. On the other hand, To construct the response surfaces by using the gPC algorithm based on the stochastic collocation method, the approximation order P is also set to three and the accuracy level l is set to three. Accordingly, the number of collocation points is 163 for 9 random variables. Therefore, 163 optimal control problems starting from the different initial states are solved for constructing the response surfaces.

In addition, we consider the randomly generated 100 different cases of the initial states as the inputs of the response surfaces. The near-optimal solution generated by using the response surfaces and the optimal solution obtained by actu-

ally solving the optimal control problem are compared with each other. Through the numerical simulations, the effectiveness and performance of our proposed response surface method for generating the near-optimal conflict-free trajectory are evaluated and demonstrated.

4.3.2 Simulation Results of Near-Optimal Conflict-Free Trajectory Generation

The near-optimal conflict-free trajectories starting from any given initial states are generated from the response surfaces constructed by using the gPC algorithm. As mentioned in section 3, by evaluating the convergence of the distance between two subsequent coefficients $\|\boldsymbol{C}^{*(Q+1)} - \boldsymbol{C}^{*(Q)}\|_\infty$, the number of sample points Q can be determined. As an example, Fig. 7 shows the distance $\|\boldsymbol{C}^{*(Q+1)} - \boldsymbol{C}^{*(Q)}\|_\infty$ using the coefficients for the terminal time of aircraft 1 t_{f1} with different numbers of sample points Q. As shown in Fig. 7, the distance $\|\boldsymbol{C}^{*(Q+1)} - \boldsymbol{C}^{*(Q)}\|_\infty$ converges after $Q = 25$, and the increase in Q does not provide significant improvements and changes in the coefficients $\boldsymbol{C}$. Thus, 25 sample
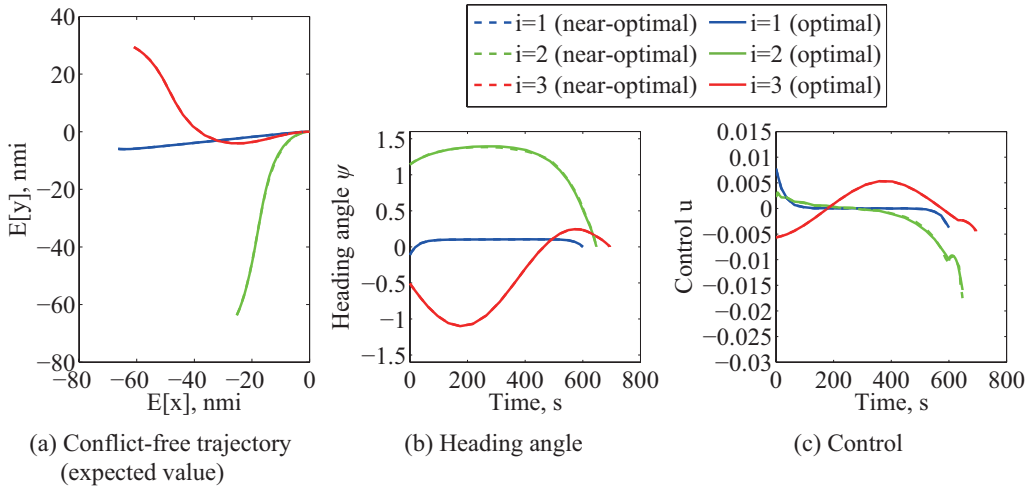
(a) Conflict-free trajectory
(expected value)

(b) Heading angle

(c) Control

Fig. 8 Near-optimal and optimal conflict-free trajectories (expected values) and dynamic variables in case 1 (worst case in x_1).

(a) Conflict-free trajectory
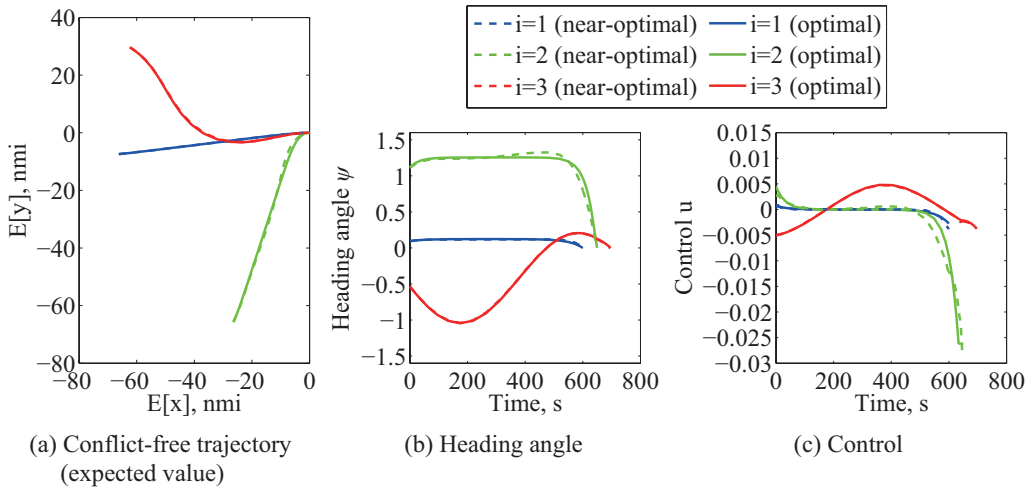(expected value)

(b) Heading angle

(c) Control

Fig. 9 Near-optimal and optimal conflict-free trajectories (expected values) and dynamic variables in case 2 (worst case in $y_1, \psi_1, t_{f2}, t_{f3}$).
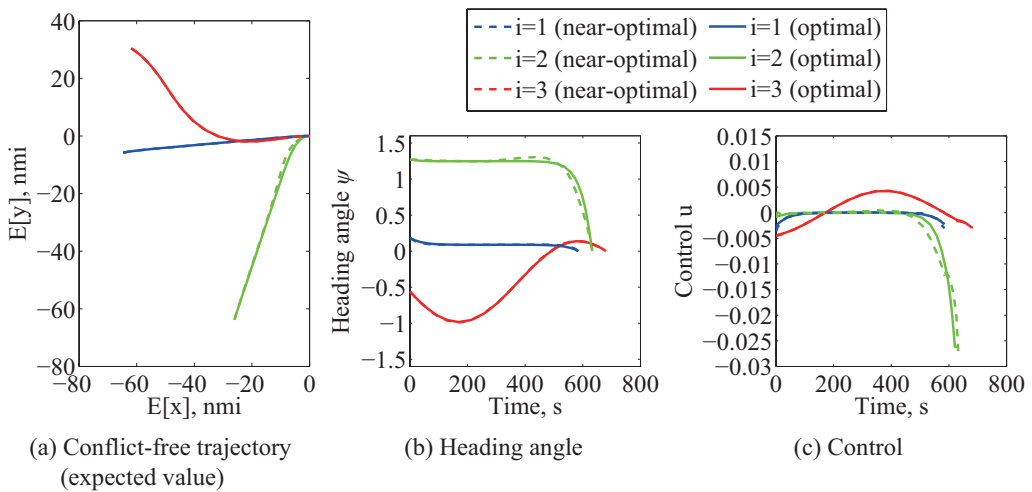

(a) Conflict-free trajectory
(expected value)

(b) Heading angle

(c) Control

Fig. 10 Near-optimal and optimal conflict-free trajectories (expected values) and dynamic variables in case 3 (worst case in x_2, y_2, ψ_2, u_2).

(a) Conflict-free trajectory
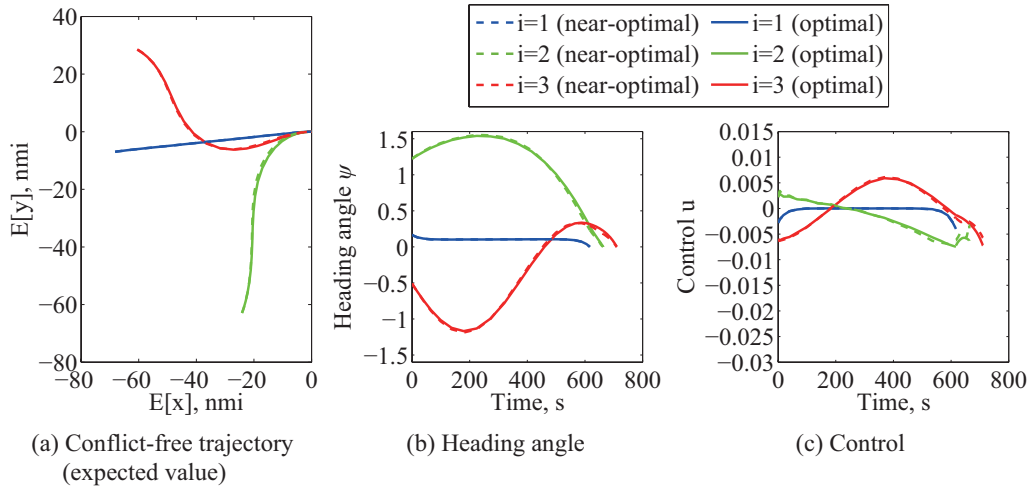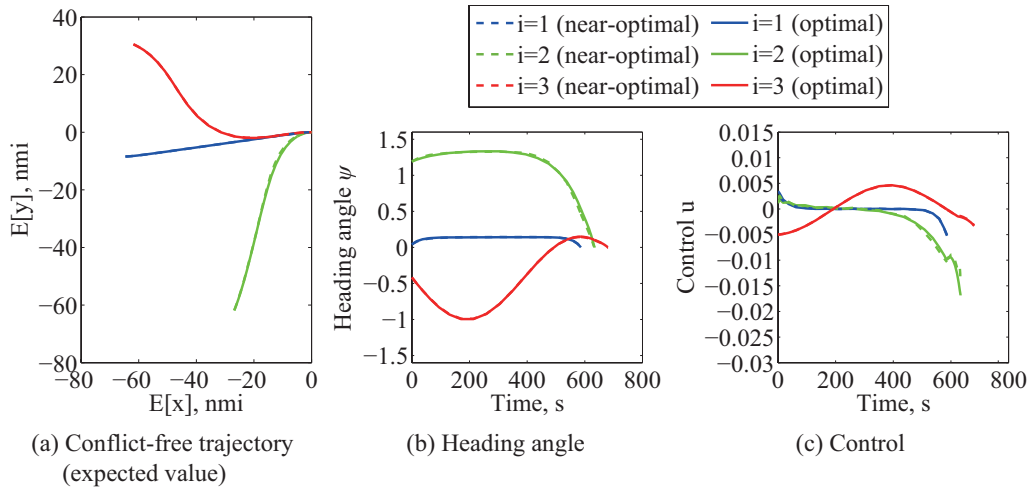(expected value)

(b) Heading angle

(c) Control

Fig. 11 Near-optimal and optimal conflict-free trajectories (expected values) and dynamic variables in case 4 (worst case in x_3, y_3, ψ_3, u_3).

(a) Conflict-free trajectory
(expected value)

(b) Heading angle

(c) Control

Fig. 12 Near-optimal and optimal conflict-free trajectories (expected values) and dynamic variables in case 5 (worst case in u_1).

(a) Conflict-free trajectory
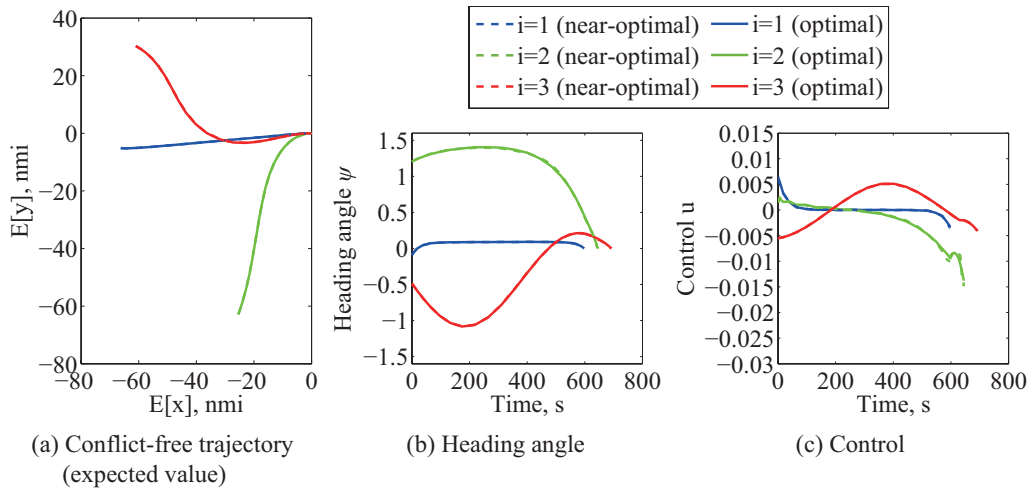(expected value)

(b) Heading angle

(c) Control

Fig. 13 Near-optimal and optimal conflict-free trajectories (expected values) and dynamic variables in case 6 (worst case in t_{f1}).

Table 5 Minimum distances between aircraft (expected values) in worst cases (case 1: worst case in x_1; case 2: worst case in $y_1, \psi_1, t_{f2}, t_{f3}$; case 3: worst case in x_2, y_2, ψ_2, u_2; case 4: worst case in x_3, y_3, ψ_3, u_3; case 5: worst case in u_1; case 6: worst case in t_{f1}).

Cases	Pairs	Near-optimal	Optimal
1	C_{12} (aircraft 1 and 2)	5.16 nmi	5.15 nmi
	C_{13} (aircraft 1 and 3)	9.76 nmi	9.74 nmi
	C_{23} (aircraft 2 and 3)	5.23 nmi	5.22 nmi
2	C_{12}	5.22 nmi	5.29 nmi
	C_{13}	10.22 nmi	10.38 nmi
	C_{23}	5.23 nmi	5.24 nmi
3	C_{12}	5.21 nmi	5.15 nmi
	C_{13}	10.44 nmi	10.42 nmi
	C_{23}	5.24 nmi	5.24 nmi
4	C_{12}	5.18 nmi	5.15 nmi
	C_{13}	8.77 nmi	8.58 nmi
	C_{23}	5.18 nmi	5.20 nmi
5	C_{12}	5.15 nmi	5.14 nmi
	C_{13}	10.41 nmi	10.43 nmi
	C_{23}	5.25 nmi	5.25 nmi
6	C_{12}	5.18 nmi	5.16 nmi
	C_{13}	9.88 nmi	9.86 nmi
	C_{23}	5.24 nmi	5.24 nmi

points are enough to apply the gPC algorithm based on convex optimization and construct the response surfaces, whereas the gPC algorithm based on the stochastic collocation method uses 163 collocation points, described in section 4.3.1.

In addition, Table 4 indicates the maximum and RMS errors between the near-optimal and optimal solutions among 100 different cases of the initial states, and the near-optimal solutions are generated from the response surfaces constructed by using the gPC algorithms based on convex optimization and the stochastic collocation method. Table 4 also shows the comparison between the errors of the response surfaces constructed by using those two gPC algorithms. As shown in Table 4, the maximum and RMS errors obtained by using convex optimization are much smaller than those obtained by employing the stochastic collocation method, which are small enough to suggest that the response surfaces constructed by using the gPC algorithm based on convex optimization have good approximation accuracy. It indicates that the gPC algo-

rithm based on convex optimization can construct the response surfaces much more accurately with a considerably smaller number of sample points than the gPC algorithm based on the stochastic collocation method.

Furthermore, Figs. 8–13 show the expected values of the near-optimal and optimal conflict resolution trajectories and the time histories of the near-optimal and optimal states and controls in the worst cases among 100 cases. The worst cases are referred to the simulation cases in which the errors in the states, controls and terminal time are maximum among 100 cases shown in Table 4: case 1 (worst case in x_1), case 2 (worst case in y_1, ψ_1, t_{f2} and t_{f3}), case 3 (worst case in x_2, y_2, ψ_2 and u_2), case 4 (worst case in x_3, y_3, ψ_3 and u_3), case 5 (worst case in u_1) and case 6 (worst case in t_{f1}). In Figs. 8–13, the blue, green and red lines indicate the solutions of aircraft 1, 2 and 3 ($i = 1$–3), respectively. The solid lines denote the optimal solutions obtained by actually solving the stochastic optimal control problems. The dashed lines are the near-optimal solutions

generated from the response surfaces, which are constructed by using the gPC algorithm based on convex optimization. As shown in Figs. 8–13, the near-optimal and optimal solutions closely match each other even though in worst cases. Moreover, Table 5 indicates the minimum distances between aircraft in the worst cases. The minimum distances in the near-optimal and optimal solutions are almost the same, and the minimum distances in the near-optimal solutions as well as the optimal solutions are larger than the minimum separation requirement of 5 nmi and can have the margins from the minimum allowed separation. In addition, the stochastic safety constraint described in Eqs. (15) and (23) are also satisfied. It indicates that the near-optimal solutions are guaranteed to avoid the potential conflicts without actually solving the optimal control problems.

Consequently, the gPC algorithm based on convex optimization can construct the response surfaces with a considerably small number of sample points, and the response surfaces provide the accurate approximate optimal conflict-free trajectories that are guaranteed to avoid potential conflicts without actually solving the stochastic optimal control problems and sacrificing accuracy. Through the numerical simulations, the effectiveness and performance of our proposed response surface method for generating the near-optimal conflict-free trajectories are evaluated and demonstrated.

5   Conclutions

In this study, we proposed the near-optimal conflict-free trajectory generation algorithm by using the generalized polynomial chaos (gPC) method. First, the computationally efficient probabilistic conflict detection and resolution algorithms were proposed by employing the gPC method based on the stochastic collocation method. As to the uncertainty during flight, the spatially correlated wind error was considered, and the Karhunen-Loeve expansion was used to describe the correlated wind error. To detect possible conflicts, the statistical information of the distance between aircraft was calculated accurately by employing the gPC algorithm, and the

conflict probability between aircraft was computed by the probabilistic conflict detection algorithm. The gPC algorithm performed much faster than the Monte Carlo (MC) method, and using the MC method especially within the iterative optimization process such as the optimal control problem for conflict resolution is computationally laborious and intractable. In addition, the stochastic optimal control method combining the computationally efficient probabilistic conflict detection algorithm into the pseudospectral method was applied to the conflict resolution problem among multiple aircraft. The stochastic algorithm could generate the effective optimal conflict-free trajectories under the wind uncertainty. Furthermore, the response surface methodology for generating the optimal conflict-free trajectories was proposed by using the gPC algorithm based on convex optimization. The gPC algorithm based on convex optimization could construct the response surfaces much more accurately with a considerably smaller number of sample points than the gPC algorithm based on the stochastic collocation method. By constructing the response surfaces, the near-optimal conflict-free trajectories starting from any given initial states under the wind uncertainty could be generated in real time, which were guaranteed to avoid potential conflicts, without actually solving the stochastic optimal control problems and sacrificing accuracy. Consequently, through the numerical simulations, the performance and effectiveness of the stochastic algorithms were evaluated and demonstrated.

To further improve the stochastic algorithms, our proposed approach is currently being extended for the three-dimensional conflict resolution problem among multiple heterogeneous aircraft. In particular, we will consider the conflicts in the three-dimensional terminal airspace in which the aircraft coming from different directions merge to the final approach fix to be aligned for landing.

Promotion of Science.

Contact Author Email Address

mailto: 0669922514@mail.ecc.u-tokyo.ac.jp

References

[1] International Civil Aviation Organization. Global Air Traffic Management Operational Concept. Doc 9854AN/458, 2005.

[2] Federal Aviation Administration Joint Planning and Development Office. Concept of Operations for the Next Generation Air Transportation System Ver. 3.2. 2010.

[3] SESAR Joint Undertaking. European ATM Master Plan Edition 2. 2012.

[4] Ministry of Land, Infrastructure, Transport and Tourism Study Group for the Future Air Traffic Systems. Long-term Vision for the Future Air Traffic Systems — Changes to Intelligent Air Traffic Systems —. 2010.

[5] Kuchar J and Yang L. A review of conflict detection and resolution methods. *IEEE Transactions on Intelligent Transportation Systems*, Vol. 1, No. 4, pp 179–189, 2000.

[6] Erzberger H, Paielli R, Isaacson D and Eshow M. Conflict detection and resolution in the presence of prediction error. *1st USA/Europe Air Traffic Management R&D Seminar*, Saclay, France, 1997.

[7] Paielli R and Erzberger H. Conflict probability estimation for free flight. *Journal of Guidance, Control, and Dynamics*, Vol. 20, No. 3, pp 588–596, 1997.

[8] Yang L and Kuchar J. Prototype conflict alerting system for free flight. *Journal of Guidance, Control, and Dynamics*, Vol. 20, No. 4, pp 768–773, 1997.

[9] Prandini M, Hu J, Lygeros J and Sastry S. A probabilistic approach to aircraft conflict detection. *IEEE Transactions on Intelligent Transportation Systems*, Vol. 1, No. 4, pp 199–220, 2000.

[10] Hu J, Prandini M and Sastry S. Aircraft conflict prediction in the presence of a spatially correlated wind field. *IEEE Transactions on Intelligent Transportation Systems*, Vol. 6, No. 3, pp 326–340, 2005.

[11] Chaloulos G and Lygeros J. Effect of wind correlation on aircraft conflict probability. *Journal of Guidance, Control, and Dynamics*, Vol. 30, No. 6, pp 1742–1752, 2007.

[12] Liu W and Hwang I. Probabilistic trajectory prediction and conflict detection for air traffic control. *Journal of Guidance, Control, and Dynamics*, Vol. 34, No. 6, pp 1779–1789, 2011.

[13] Lecchini-Visintini A, Glover W, Lygeros J and Maciejowski J M. Monte Carlo optimization for conflict resolution in air traffic control. *IEEE Transactions on Intelligent Transportation Systems*, Vol. 7, No. 4, pp 470–482, 2006.

[14] Kantas N, Lecchini-Visintini A and Maciejowski J M. Simulation-based Bayesian optimal design of aircraft trajectories for air traffic management. *International Journal of Adaptive Control and Signal Processing*, Vol. 24, pp 882–899, 2010.

[15] Liu W and Hwang I. Probabilistic aircraft midair conflict resolution using stochastic optimal control. *IEEE Transactions on Intelligent Transportation Systems*, Vol. 15, No. 1, pp 37–46, 2014.

[16] Cole R, Richard C, Kim S and Bailey D. An Assessment of the 60 km Rapid Update Cycle (RUC) with Near Real-Time Aircraft Reports. Project Report NASA/A-1, MIT Lincoln Laboratory, Lexington, 1998.

[17] Xiu D and Karniadakis G E. The Wiener–Askey polynomial chaos for stochastic differential equations. *SIAM Journal on Scientific Computing*, Vol. 24, No. 2, pp 619–644, 2002.

[18] Xiu D and Hesthaven J S. High-order collocation methods for differential equations with random inputs. *SIAM Journal on Scientific Computing*, Vol. 27, No. 3, pp 1118–1139, 2005.

[19] Xiu D. *Numerical Methods for Stochastic Computations*. Princeton University Press, Princeton, 2010.

[20] Patterson M A and Rao A V. Exploiting sparsity in direct collocation pseudospectral methods for solving optimal control problems. *Journal of Spacecraft and Rockets*, Vol. 49, No. 2, pp 364–377, 2012.

[21] Ghosh P and Conway B A. Near-optimal feedback strategies synthesized using a spatial statistical approach. *Journal of Guidance, Control, and Dynamics*, Vol. 36, No. 4, pp 905–919,

2013.

[22] Fagiano L and Khammash M. Simulation of stochastic systems via polynomial chaos expansions and convex optimization. *Physical Review E*, Vol. 86, 036702, 2012.

[23] Boyd S and Vandenberghe L. *Convex Optimization*. Cambridge University Press, New York, 2009.

[24] Schwartz B, Benjamin S, Green S and Jardin M. Accuracy of RUC-1 and RUC-2 wind and aircraft trajectory forecasts by comparison with ACARS observations. *Weather and Forecasting*, Vol. 15, No. 3, pp 316–326, 2000.

[25] Ghanem R G and Spanos P D. *Stochastic Finite Elements: A Spectral Approach*. Springer-Verlag, New York, 1991.

[26] International Civil Aviation Organization. Procedures for Air Navigation Services Air Traffic Management. Doc 4444ATM/501, 2007.

[27] Smolyak S A. Quadrature and interpolation formulas for tensor products of certain classes of functions. *Soviet Mathematics*, Vol. 4 pp 240–243, 1963.

[28] Heiss F and Winschel V. Likelihood approximation by numerical integration on sparse grids. *Journal of Econometrics*, Vol. 144, No. 1, pp 62–80, 2008.

[29] Schwarm A and Nikolaou M. Chance-constrained model predictive control. *AlChE Journal*, Vol. 45, pp 1743–1752, 1999.

[30] Blackmore L, Ono M, Bektassov A and Williams B C. A probabilistic particle-control approximation of chance-constrained stochastic predictive control. *IEEE Transactions on Robotics*, Vol. 26, No. 3, pp 502–517, 2010.

[31] Rao A V, Benson D, Darby C L, Mahon B, Francolin C, Patterson M, Sanders I and Huntington G T. User's Manual for GPOPS Version 5.0: A MATLAB Software for Solving Multiple-Phase Optimal Control Problems Using hp-Adaptive Pseudospectral Methods. University of Florida, Gainesville, 2011.

[32] Gill P E, Murray W and Saunders M A. SNOPT: an SQP algorithm for large-scale constrained optimization. *SIAM Review*, Vol. 47, No. 1, pp 99–131, 2005.

[33] Grant M and Boyd S. CVX: matlab software for disciplined convex programming, version 1.22. URL: http://cvxr.com/cvx/, 2012.

[34] Grant M and Boyd S. Graph implementations for nonsmooth convex programs. *Recent Advances in Learning and Control*, Edited by Blondel V, Boyd S and Kimura H, pp 95–110, 2008.

Copyright Statement